ISSN (Print) 1226-1750
ISSN (Online) 2233-6656
Journal of Magnetics 18(3), 240-244 (2013) http://dx.doi.org/10.4283/JMAG.2013.18.3.240

Magnetic Microstructures and Corrosion Behaviors of Nd-Fe-B-Ti-C Alloy by Ga Doping

Qiong Wu[1], Pengyue Zhang[1]*, Hongliang Ge[1], Aru Yan[2], and Dongyun Li[1]

[1]China Jiliang University, Magnetism Key Laboratory of Zhejiang Province, Hangzhou 310018, China
[2]Key Laboratory of Magnetic Materials and Devices, Ningbo Institute of Material Technology & Engineering, Chinese Academy of Sciences, Ningbo 315201, China

(Received 6 March 2013, Received in final form 21 May 2013, Accepted 10 June 2013)

The influences of Gallium doping on the magnetic microstructures and corrosion behaviors of Nd-Fe-B-Ti-C alloys are investigated. The cooling rate for obtaining fully amorphous structure is raised, and the glass-forming ability is improved by the Ga addition. The High Resolution Transmission Electron Microscopy image shows that the α-Fe and Fe_3B soft magnetic phases become granular surrounded by the $Nd_2Fe_{14}B$ hard magnetic phase. The rms and $(\Delta\varphi)_{rms}$ value of Nd-Fe-B-Ti-C nanocomposite alloy thick ribbons in the typical topographic and magnetic force images detected by Magnetic Force Microscopy(MFM) decreases with 0.5 at% Ga addition. The corrosion resistances of $Nd_9Fe_{73}B_{12.6}C_{1.4}Ti_{4-x}Ga_x$ (x = 0, 0.5, 1) alloys are enhanced by the Ga addition. It can be attributed to the formation of more amorphous phases in the Ga doped samples.

Keywords: nanocomposite rare-earth magnets, microstructures, corrosion behaviors

1. Introduction

Recent investigations have shown that, excellent hard magnets with large coercivity can be obtained in Nd-Fe-B-Ti-C nanocomposite alloys in a composition of Nd content from 6-9 atomic percent and B content from 10-15 atomic percent, in which Titanium addition suppresses α-Fe and metastable $Nd_2Fe_{23}B_3$ phase and Carbon addition refines grain, and suppresses unfavorable formation of TiB_2 [1, 2]. One of outstanding characteristics of this type of material is great glass-forming ability [3, 4], which allows strip casting (SC) method to mass-produce this type of alloy powder with a higher production efficiency and a lower cooling rate compared to melt spinning method [5-7]. However, the cooling rate required for Nd-Fe-B-Ti-C nanocomposite alloys is not enough low to obtain large coercivity by means of the strip casting (SC) process because of grain coarsening [8]. Further improvement of cooling-rate dependency of the alloys and grain refinement is important for increasing the coercivity. Rintaro Ishii *et al.* [9] have reported that influences of various elements (Ti, Nb, Mo, Ta, Hf, W, V, Cr) on magnetic properties of Fe-B/$Nd_2Fe_{14}B$-based Nd-Fe-B-Ti-C nanocomposite magnets in order to obtain larger coercivity. In our previous study, Ga addition is effective to improve the glass-forming ability (GFA) and to enhance the magnetic properties. By adding 0.5 at% Ga, high performance of magnetic properties with the coercivity about 1120 kA/m was obtained even at such a low cooling rate with v_s (surface velocity of quenching) of 5 m/s [10].

In addition, an understanding of the corrosion behavior is necessary for practical application of Nd-Fe-B-Ti-C nanocomposite alloy. However, little work has been done on this topic for this type alloy. In this paper, cooling-rate dependence of the Ga-added Nd-Fe-B-Ti-C nanocomposite alloys was discussed further. And the effects of Gallium doping on the corrosion behavior of Nd-Fe-B-Ti-C thick ribbons with low cooling rate was investigated in detail.

2. Experimental Details

The alloy ingots with nominal compositions of $Nd_9Fe_{73}B_{12.6}C_{1.4}Ti_{4-x}Ga_x$ (x = 0, 0.5, 1) were obtained by arc melting mixtures of Nd, Fe, Ti, C with a purity of more than 99.9% and pre-alloyed FeB in argon atmosphere. In order to obtain a homogeneous alloy ingot, the alloy melting conditions are as follows: Firstly, the alloy was melted two times; secondly, the alloy ingot was then

©The Korean Magnetics Society. All rights reserved.
*Corresponding author: Tel: +86-571-87676292
Fax: +86-571-28889526, e-mail: wuqiong@cjlu.edu.cn

© 2013 Journal of Magnetics

flipped, and melted two times again; after cooling, the alloy ingot was then taken out, and crushed into small pieces, and steps 1 and 2 was repeated. Melt-spinning was performed by inductively heating crushed arc-melted ingots in a quartz crucible in an Ar atmosphere at 1300 °C. The melt was ejected through an orifice of 0.5 mm diameter onto a rapidly rotating copper wheel with various surface speeds. Especially, $Nd_9Fe_{73}B_{12.6}C_{1.4}Ti_{4-x}Ga_x$ (x = 0, 0.5, 1) thick ribbons of thickness about 300-500 ìm were prepared by rapidly solidification technique at v_s of 5 m/s. These ribbons were annealed isothermally under vacuum environment in a tubular furnace at 600-750 ºC for 10 min.

The microstructure was examined by a Bruker D8 advance diffractometer X-ray diffraction (XRD) with Cu $K\alpha$ radiation and transmission electron microscopy (TEM). Magnetic measurements were accomplished by a vibrating-sample magnetometer (VSM) of Lake-Shore 7407 with a maximum applied field of 2.0 T. The magnetic microstructures on free surface of the ribbons were detected by a magnetic force microscope (MFM) Nano-Scope IIIa-D3000 in Tapping/Lift modes with the tip lift-height of 20-50 nm. Prior to MFM measurements, the ribbons were heat treated at 400 ºC under vacuum of 1×10^{-4} Pa for 3 h to remove the stress in the surface during the process. In order to detect the permanent magnetic specimen clearly, high coercivity of about 75 kA/m Co-Cr coated tips were used. Electrochemical measurements were carried out using a typical three-electrode system: a stationary specimen, a pair of counter electrodes (made of Pt sheet) and a saturated calomel reference electrode (SCE). An Ivium CompactStat.e10800 electrochemical workstation was used for the polarization curves measurements at room temperature after 20 min exposure to the test solution starting at the open-circuit potential. The test solution, 5.0 wt.% NaCl aqueous solution, was prepared with analytical grade NaCl reagent (≥ 99.5 wt.%) and deionized water. A scan rate of 1.0 mV/s was used for the potentiodynamic polarization test.

3. Results

Figure 1 shows XRD patterns of the as-cast melt-spun $Nd_9Fe_{73}B_{12.6}C_{1.4}Ti_{4-x}Ga_x$ (x = 0, 0.5) ribbons at v_s of 5 m/s, 10 m/s, 15 m/s and 20 m/s. The content of amorphous phase for the both samples both increases with surface velocity of copper roll. For x = 0 ribbons with v_s of 20 m/s, the crystalline peaks disappear and the diffraction pattern consists only of one broad peak, indicating that fully amorphous structure is formed. For x = 0.5 alloy, the v_s for fully amorphous structure decreases to 15 m/s. The copper roll surface velocity for fully amorphous structure is decreased, i.e. the cooling rate for fully amorphous structure is reduced, and the GFA is improved by the Ga addition. Their magnetic hysteresis loops are shown in Fig. 2(a) and (b). At v_s = 5 m/s, the coercivity increases from 760 kA/m to 1120 kA/m with 0.5 at% Ga doping. The dramatically enhancement of the coercivity is attributed to grain refinement [10].

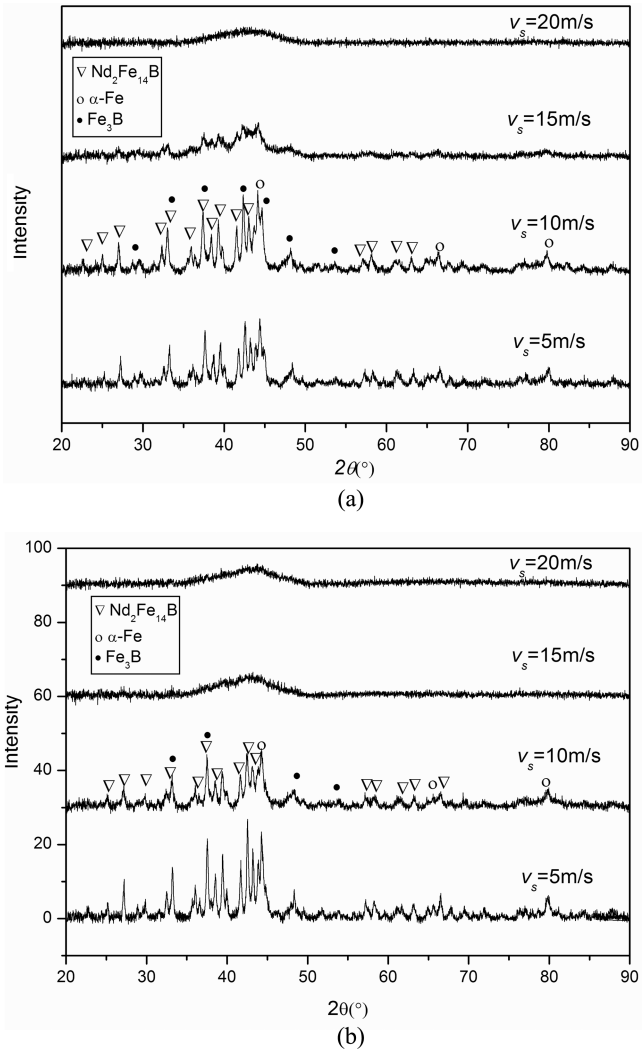

Fig. 1. XRD patterns of the as-cast melt-spun (a) x = 0 and (b) x = 0.5 ribbons at v_s of 5 m/s, 10 m/s, 15 m/s and 20 m/s.

The High Resolution Transmission Electron Microscopy (HRTEM) image and corresponding electron diffraction pattern of x = 0.5 thick ribbon obtained at v_s of 5 m/s is shown in Fig. 3. It can be seen from the image that the α-Fe and Fe_3B soft magnetic phases become granular surrounded by the $Nd_2Fe_{14}B$ hard magnetic phase. In our previous paper [10], the existence of exchange coupling interaction between soft and hard phases is confirmed in

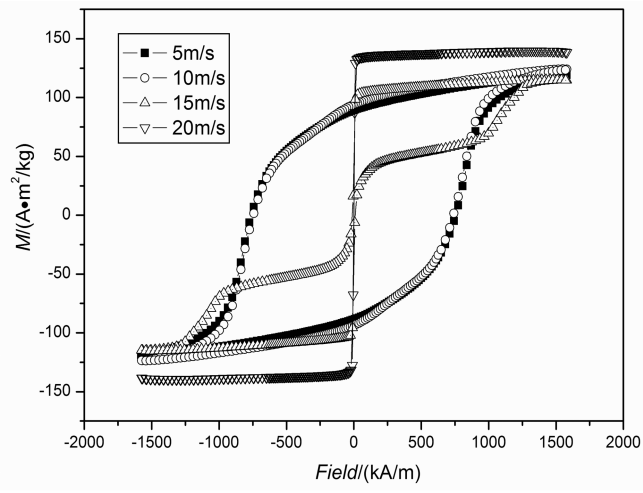

Fig. 2. Magnetic hysteresis loops of as-cast melt-spun (a) x = 0 and (b) x = 0.5 ribbons at v_s of 5 m/s, 10 m/s, 15 m/s and 20 m/s.

the $Nd_9Fe_{73}B_{12.6}C_{1.4}Ti_{4-x}Ga_x$ (x = 0, 0.5, 1) samples. The microstructure with soft magnetic phases surrounded by hard magnetic phase can be in favor of exchange coupling interaction between the soft and hard magnetic phases, which is more appropriate to obtain good hard magnetic properties [1].

Figure 4 shows the typical topographic and magnetic force images of the $Nd_9Fe_{73}B_{12.6}C_{1.4}Ti_{4-x}Ga_x$ (x = 0, 0.5) thick ribbons at v_s =5 m/s. The scan size of all images is 5 μm × 5 μm. It is seen in Fig. 4(b) and (d) that the root-mean-square (rms) roughness of the $Nd_9Fe_{73}B_{12.6}C_{1.4}Ti_{3.5}Ga_{0.5}$ ribbon is far smaller than $Nd_9Fe_{73}B_{12.6}C_{1.4}Ti_4$ without Ga, which consists of many large crystals. As is shown in Fig. 4(a) and (c), the magnetic force images are characterized by adjacent bright or dark spots (domains)

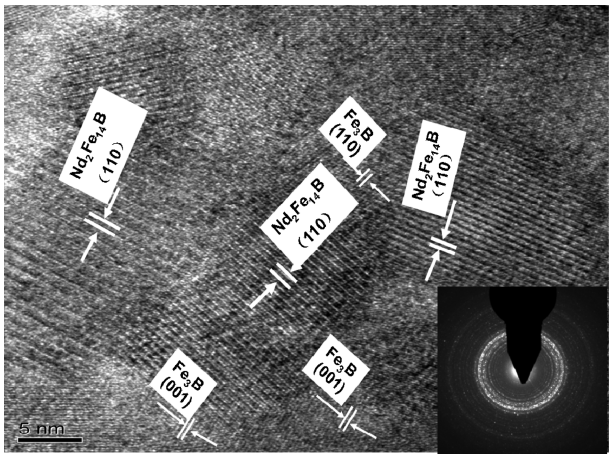

Fig. 3. High-resolution transmission electron microscopic image and corresponding electron diffraction pattern of $Nd_9Fe_{73}B_{12.6}C_{1.4}Ti_{3.5}Ga_{0.5}$ x = 0.5 thick ribbons at v_s of 5 m/s.

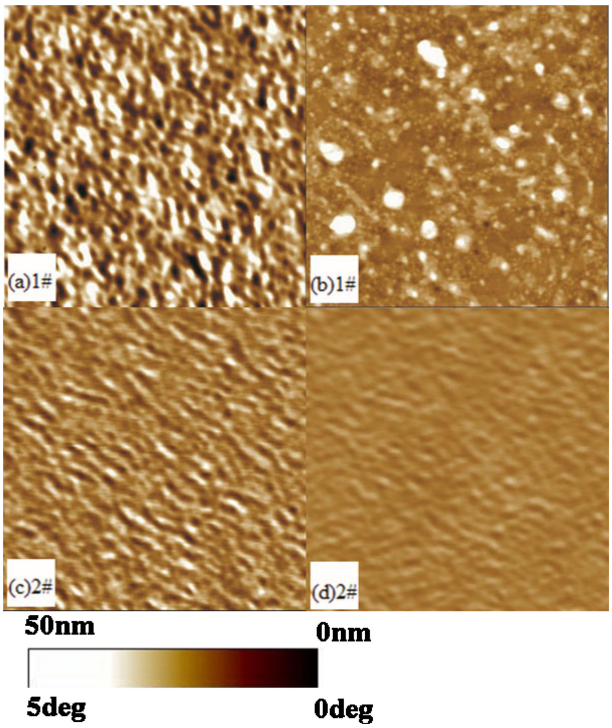

Fig. 4. (Color online) The magnetic force images (a) (c) (scan size: 5 μm × 5 μm, data scale: 50 nm) and the topographic images of (b) (d) (scan size: 5 μm × 5 μm, data scale: 5°) x = 0 (1#) and x = 0.5 (2#) ribbons at v_s = 5 m/s.

in submicron scale and random distribution. For a downward magnetized tip, bright or dark spots imply that t heir corresponding magnetic moment is upward or downward, respectively. The values of root-mean-square (rms) roughness of phase shift $(\Delta\varphi)_{rms}$ is defined as $(\Delta\varphi)_{rms}$ =

$\sqrt{\frac{\sum_{i=1}^{N}(\varphi_i - \varphi_{ave})^2}{N}}$, where φ_{ave} is the average φ value within the given area, φ_i is the current φ value, and N is the number of points within a given area. The $(\Delta\varphi)_{rms}$ value reflects the contrast of bright and dark domains, which decreases from 0.49° to 0.37° with 0.5 at% Ga by comparing Fig. 4(c) with Fig. 4(a). The XRD results have confirmed that the GFA of $Nd_9Fe_{73}B_{12.6}C_{1.4}Ti_4$ alloy is enhanced by Ga addition. Comparing to the ribbons without Ga addition, the $Nd_9Fe_{73}B_{12.6}C_{1.4}Ti_{3.5}Ga_{0.5}$ thick ribbons may possess more amorphous phase at the same various surface speeds of copper wheel. It can be explained that the smaller rms and $(\Delta\varphi)_{rms}$ value of $Nd_9Fe_{73}B_{12.6}C_{1.4}Ti_{3.5}Ga_{0.5}$ ribbon.

The influence of Ga addition on corrosion behaviors of Nd-Fe-B-Ti-C alloys is discussed also. The corrosion resistances of $Nd_9Fe_{73}B_{12.6}C_{1.4}Ti_{4-x}Ga_x$ (x = 0, 0.5, 1) alloys are characterized by gain weights of ribbons under certain aging conditions. Figure 5 shows histogram of gain weight for as-cast melt-spun $Nd_9Fe_{73}B_{12.6}C_{1.4}Ti_{4-x}Ga_x$ (x = 0, 0.5, 1) thick ribbons at v_s = 5 m/s under T = 120 °C and HR= 95% for 192 hours. It is turned out that gain weights of as-cast melt-spun $Nd_9Fe_{73}B_{12.6}C_{1.4}Ti_{4-x}Ga_x$ (x = 0, 0.5, 1) thick ribbons decrease with the Ga content, indicating that the corrosion resistance is enhanced by the Ga addition.

The typical potentiodynamic polarization curves of as-cast melt-spun $Nd_9Fe_{73}B_{12.6}C_{1.4}Ti_{4-x}Ga_x$ (x = 0, 0.5, 1) thick ribbons, obtained in 5 wt% NaCl solution open to air at 298 K, are shown in Fig. 6. As can be observed, the polarization curves are well defined, having an activation-controlled region where the current density changes exponentially with electrode potential. The results of corrosion

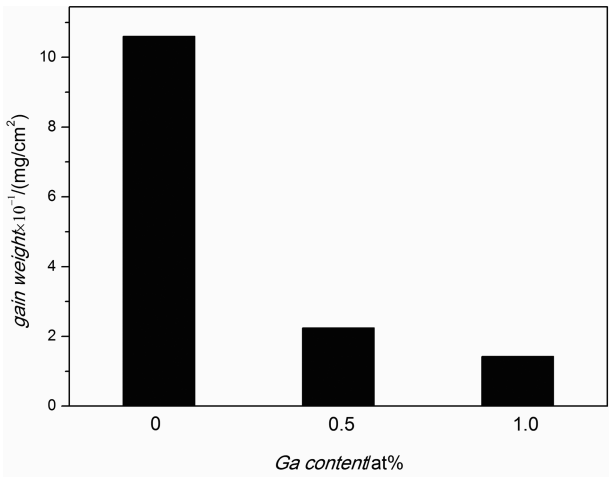

Fig. 5. Gain weights of as-cast melt-spun $Nd_9Fe_{73}B_{12.6}C_{1.4}Ti_{4-x}Ga_x$ (x = 0, 0.5, 1) thick ribbons at v_s = 5 m/s under T = 120 °C and HR = 95% for 192 hours.

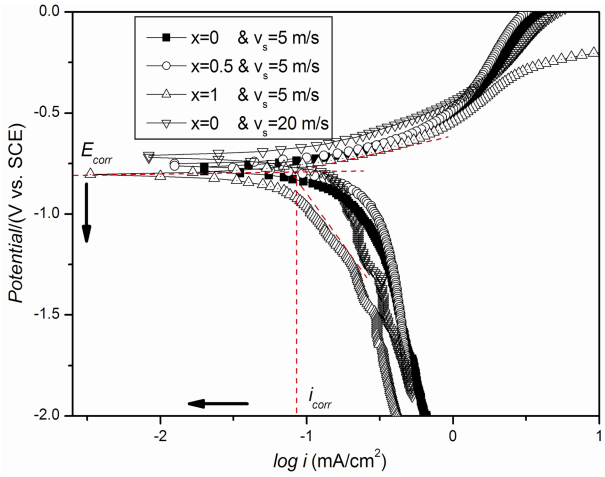

Fig. 6. (Color online) Potentiodynamic polarization curves of as-cast melt-spun $Nd_9Fe_{73}B_{12.6}C_{1.4}Ti_{4-x}Ga_x$ (x = 0, 0.5, 1) thick ribbons at v_s = 5 m/s and $Nd_9Fe_{73}B_{12.6}C_{1.4}Ti_{4-x}Ga_x$ (x = 0) ribbons at v_s = 20 m/s in 5 wt% NaCl solution.

Table 1. E_{corr} and i_{corr} of as-cast melt-spun $Nd_9Fe_{73}B_{12.6}C_{1.4}Ti_{4-x}Ga_x$ (x = 0, 0.5, 1) thick ribbonsn 5% NaCl solution.

Ga content	v_s (m/s)	E_{corr}/V	$i_{corr} \times 10^{-4}$/(A/cm^2)
$x = 0$	5	–0.7766	2.952
$x = 0.5$	5	–0.7838	2.775
$x = 1.0$	5	–0.7613	1.326
$x = 0$	20	–0.6404	1.187

potential (E_{corr}) and corrosion current density (i_{corr}) are summarized in Table 1. The i_{corr} determined from the intersection of extrapolated cathodic and anodic Tafel lines at the corrosion potential for all the samples. The E_{corr} remains almost constant with increasing the Ga content up to 1 at%. However, the i_{corr} shows a sharp reduction with the 1at% Ga addition from 2.952×10^{-4}A/cm^2 to 1.326×10^{-4} A/cm^2. Generally, smaller i_{corr} means higher corrosion resistance [14]. The results from the typical potentiodynamic polarization curves further prove that the corrosion resistance of Nd-Fe-B-Ti-C alloys is enhanced by the Ga addition.

The typical potentiodynamic polarization curve of the fully amorphous $Nd_9Fe_{73}B_{12.6}C_{1.4}Ti_{4-x}Ga_x$ (x = 0) ribbons at v_s = 20 m/s is also presented in Fig. 6. And the results of E_{corr} and i_{corr} of the fully amorphous sample are summarized in Table 1. Comparing to as-cast melt-spun $Nd_9Fe_{73}B_{12.6}C_{1.4}Ti_{4-x}Ga_x$ (x = 0) thick ribbons at v_s = 5 m/s with crystalline phases, including $Nd_2Fe_{14}B$, α-Fe and Fe_3B phase, the E_{corr} of the fully amorphous sample increases from –0.7766 V to –0.6404 V, and i_{corr} decreases from 2.952×10^{-4} A/cm^2 to 1.187×10^{-4} A/cm^2, indicating that the fully amorphous sample of $Nd_9Fe_{73}B_{12.6}C_{1.4}$-

$Ti_{4-x}Ga_x$ (x = 0) alloy possesses higher corrosion resistance. Improved corrosion behavior by Ga addition can be explained by the formation of more amorphous phases.

4. Conclusions

$Nd_9Fe_{73}B_{12.6}C_{1.4}Ti_{4-x}Ga_x$ (x = 0, 0.5, 1) ribbons were prepared by melt spinning technique at various surface speeds. The influence of Gallium doping on the magnetic microstructure and corrosion behaviors of Nd-Fe-B-Ti-C alloys were investigated. The results of XRD for the as-spun $Nd_9Fe_{73}B_{12.6}C_{1.4}Ti_{4-x}Ga_x$ (x =0, 0.5) ribbons at various surface speeds showed the cooling rate for fully amorphous structure was raised, and the GFA was improved by the Ga addition. It was found that the α-Fe and Fe_3B soft magnetic phases become granular surrounded by the $Nd_2Fe_{14}B$ hard magnetic phase from the HRTEM image. The magnetic microstructures detected by MFM revealed that the rms and $(\Delta\varphi)_{rms}$ value of Nd-Fe-B-Ti-C nanocomposite alloy thick ribbons was decreased with 0.5 at% Ga addition. The corrosion resistances of $Nd_9Fe_{73}B_{12.6}C_{1.4}Ti_{4-x}Ga_x$ (x = 0, 0.5, 1) alloys were enhanced by the Ga addition. The GFA was improved by the Ga doping, which caused the formation of amorphous phases in the x = 1 sample. The amorphous phases enhanced corrosion resistances, but deteriorated the magnetic properties.

Acknowledgments

This work was supported by Project of Zhejiang Province Innovative Research Team (No. 2010R50016), the Provincial Natural Science Foundation (No. LQ12E01006), National natural Science Foundation of China (No. 51001092) and National public interest research special (No. 201210107).

References

[1] S. Hirosawa, H. Kanekiyo, and T. Miyoshi, J. Magn. Magn. Mater. **281**, 58 (2004).
[2] S. Hirosawa, H. Kanekiyo, T. Miyoshi, K. Murakami, Y. Shigemoto, and T. Nishiuchi, IEEE Trans. Magn. **40**, 2883 (2004).
[3] D. J. Branagan and R. W. McCallum, J. Alloy. Compd. **218**, 143 (1995).
[4] D. J. Branagan and R. W. McCallum, J. Alloy. Compd. **244**, 40 (1996).
[5] S. Hirosawa, Y. Shigemoto, T. Miyoshi, and H. Kanekiyo, Scr. Mater. **48**, 839 (2003).
[6] R. Coehoorn, D. B. Mooij, and C. de Waard, J. Magn. Magn. Mater. **80**, 101 (1989).
[7] S. Hirosawa, H. Kanekiyo, T. Miyoshi, Y. Shigemoto, K. Murakami, Y. Senzaki, and T. Nishiuchi, J. Alloy. Compd. **408**, 260 (2006).
[8] T. Miyoshi, H. Kanekiyo, and S. Hirosawa, IEEE Trans. Magn. **41**, 3865 (2005).
[9] R. Ishii, T. Miyoshi, H. Kanekiyo, and S. Hirosawa, J. Magn. Magn. Mater. **312**, 410 (2007).
[10] Q. Wu, T. Yu, S. Guo, X. C. Feng, M. X. Pan, P. Y. Zhang, B. S. Han, H. L. Ge, and A. R. Yan. J. Appl. Phys. **111**, 07A730 (2012).